Improvement of Fatigue Strength of Additively Manufactured Aluminum Alloy AlSi10Mg by Submerged Laser Peening

Hitoshi Soyama *

Posted Date: 31 July 2024

doi: 10.20944/preprints202407.2522.v1

Keywords: additive manufacturing; fatigue; post-processing; submerged laser peening; powder bed fusion (PBF); laser sintering (LS); AlSi10Mg; cavitation peening; fiber laser

Article

Improvement of Fatigue Strength of Additively Manufactured Aluminum Alloy AlSi10Mg by Submerged Laser Peening

Hitoshi Soyama

Department of Finemechanics, Tohoku University, Sendai 980-8579, Japan
* Correspondence: soyama@mm.mech.tohoku.ac.jp; Tel.: +81-22-795-6891; Fax: +81-22-795-3758

Abstract: As fatigue properties of as-built components of additively manufactured (AM) metals are considerably weaker than those of wrought metals because of rougher surface, post-processing is necessary to improve fatigue properties. To demonstrate improvement of fatigue properties of AM metals by post-processing, powder bed fusion (PBF) using laser sintering (LS) AlSi10Mg, i.e., PBF-LS/AlSi10Mg was treated by "submerged laser peening (SLP)" using a fiber laser and/or a Nd:YAG laser, then evaluated by plane bending fatigue tests. At SLP, "laser ablation (LA)" is generated by a pulsed laser, and a bubble is generated after LA, which behaves like a cavitation bubble that is named as "laser cavitation (LC)". In the present paper, LA-dominated SLP is called as "laser treatment (LT)", while LC-collapse-dominated SLP is called as "laser cavitation peening (LCP)", as impact at LC collapse is used for peening. It was revealed that SLP using the fiber laser was LT rather than LCP. It was demonstrated that the fatigue strength at $N = 10^7$ was 85 MPa for LCP, and 103 MPa for combined process of blasting (B) + LT + LCP, whereas the fatigue strength of as-built specimen was 54 MPa.

Keywords: additive manufacturing; fatigue; post-processing; submerged laser peening; powder bed fusion (PBF); laser sintering (LS); AlSi10Mg; cavitation peening; fiber laser

1. Introduction

Additive manufacturing (AM) metals are attractive metals, as they are manufactured directly from computer-aided design CAD / computer-aided manufacturing CAM [1, 2] [3-6]. However, fatigue properties of as-built AM metals are considerably weaker than those of bulk metals [7-12], as surface roughness of as-built is very rough due to partially melted particles which are used at AM process. Thus, post-processing to improve fatigue properties of as-built AM metals is required by smoothing surface and introducing compressive residual stress [9, 13-17]. As it was reported that the improvement of fatigue strength of powder bed fusion (PBF) using laser sintering (LS) titanium alloy Ti6Al4V by submerged laser peening (SLP) was better than that of shot peening (SP) and cavitation peening (CP) [12], the effect of SLP on the fatigue properties of PBF-LS/AlSi10Mg should be investigated, as the fatigue properties of PBF-LS/AlSi10Mg was considerably weak [18-22], and fatigue behavior of PBF-LS/AlSi10Mg was enhanced by post processing [15, 16, 23-32].

In case of laser peening (LP), in which a pulsed laser is used for peening, there are two major methods. One method is that the pulsed laser is irradiated to a target which is covered with a water film, i.e., LP with water film [33-41]. The other method is that the pulsed laser is irradiated to a target in water [42-47], it is called as "submerged laser peening (SLP)". At both laser peening, i.e., LP with water film and SLP, it has been believed that plastic deformation is produced by "laser ablation (LA)" with confining medium, i.e., water [48]. Note that in the case of SLP, a bubble is generated and expanded after LA, shrunk, then collapsed as similar to cavitation bubble (see Figure 1). The high-speed images in Figure 1 were cited from the reference [12] to show a typical SLP. In the present paper, the laser induced bubble is called as "laser cavitation (LC)". At LA-stage, the pulsed laser generates LA and it also produces thermal effects such as melting the surface of the specimen. At LC-collapse-stage, LC is collapsed and rebound, impact is produced at LC-collapse. When a pressure in water was measured by a submerged shock wave sensor, the amplitude of the pressure at LA was

 doi:10.20944/preprints202407.2522.v1

larger than that of LC-collapse [49, 50]. On the other hand, an impact passing through target metal was measure by using a handmade polyvinylidene fluoride PVDF sensor [50], the impact at LC-collapse is 1.3 times larger than that at LA. Namely, in the case of the impact which affects the target metals, LC-collapse is more effective than LA. Then, SLP can be distinguished by its mechanism into LA-stage and LC-collapse-stage.

As mentioned later, the pulse width t_w of the pulsed laser was changed in the present study, and the pulsed laser of longer t_w produced heat effects such as melting the surface of the target at LA-stage. It is a kind of "laser treatment (LT)", in which melting and peening due LA are included. On the other hand, at LC-collapse-stage, the impact which can be utilized for peening was generated. As a peening method using cavitation impact is called as cavitation peening (CP) [51], a peening using LC-collapse is named as "laser cavitation peening (LCP)". Thus, for the convenience in the present paper, depending on which mechanism is dominant, SLP was classified as LT or LCP as shown in Figure 1.

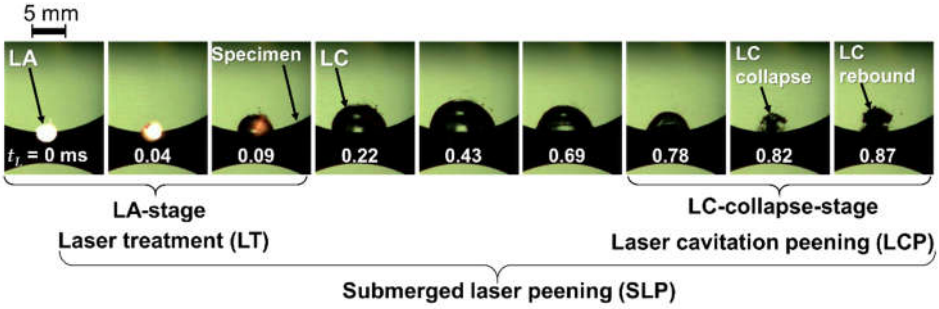

Figure 1. Typical aspect of submerged laser peening (LCP). Definition of laser ablation (LA), laser cavitation (LC), laser treatment (LT) and laser cavitation peening (LCP). The high-speed images were reprinted from [12] with permission from Elsevier, License Number 5824671356429.

As mentioned above, the fatigue properties of as-built PBF-LS/AlSi10Mg are considerably weak, and they can be enhanced by post-processing such as shot peening (SP) [23] [24, 26, 31], LP [26, 29, 30], ultrasonic surface modification [29], tumble finishing [32]. As well know, hot isostatic pressing HIP is effective method to improve fatigue properties [8] [52-59], however, HIP cannot improve the fatigue properties due to surface defect [60]. It was reported that the improvement of fatigue strength of as-built PBF-LS/TiAl4V by SLP was better than SP and CP [12] and magnesium alloy [61], Thus, in the present paper, SLP was chosen for the mechanical surface treatment for as-built PBF-LS/AlSi10Mg, as the surface smoothing and the introduction of compressive residual stress are key factors to improve the fatigue properties of as-built AM metals [11, 12, 62].

At both LP with water film and SLP, a Nd:YAG laser with Q-switch, whose pulse width t_w is several nanoseconds has been used, as LA is required at conventional LP. A typical repetition frequency of a conventional Nd:YAG laser is about dozens Hz, and several pulses/mm^2 to dozens of pulses/mm^2 is required for the improvement of the fatigue strength [12, 61]. On the other hand, a high-repetition portable pulse laser system, whose power and pulse width were 10 mJ and 1.3 ns, has been developed [46]; however, its repetition frequency is about 100 Hz, and 800–1600 pulses/mm^2 are required for treatment. Namely, the slow processing speed due to the repetition frequency of the laser system is an obstacle to the practical application of LP.

In order to increase a generation frequency of cavitation bubble, a cavitation generator using a piezo actuator has been developed [63], however, the bubble size was still too small, although vortex cavitation is key factor at CP [64]. In the view point of generation of LC at dental and medical applications, a pulsed laser with pulse width of several hundred microseconds has been used [65-68]. Of course, heat effect of the pulsed laser has been used at the surgery. It was proofed that a laser pulse of several hundreds microseconds was applicable for LCP [69]. Thus, to increase a repetition frequency of a laser system for LP, a fiber laser could be used instead of a Nd:YAG laser with Q-switch, as a fiber laser can produce laser pulses of tens to hundreds of microseconds at kHz-order.

In the present paper, in order to develop a novel post-processing using a fiber laser for the improvement of fatigue properties of as-built PBF-LS/AlSi10Mg comparing with conventional SLP, as-built PBF-LS/AlSi10Mg specimens were treated by SLP using a fiber laser and/or a Nd:YAG laser

 doi:10.20944/preprints202407.2522.v1

with Q-switch, and tested by plane bending fatigue tests. The surface characteristics such as surface roughness, residual stress and hardness were evaluated. Then, an experimental formula to estimate the improved fatigue life by SLP using the fiber laser and/or the Nd:YAG laser was proposed considering the surface roughness and the residual stress.

2. Materials and Methods

2.1. Material and Test Specimens

Figure 2 shows (a) a schematic and (b) a photograph of a specimen for the plane bending fatigue test manufactured by PBF-LS/AlSi10Mg. PBF-LS/AlSi10Mg conditions were standard condition of EOS M290 (EOS GmbH, Krailing, Germany) as follows; laser power was 400 W, laser spot diameter was 100 μm, preheating temperature of a build platform was 473 K, layer thickness was 30 μm. The used particle size was 38 – 53 μm in diameter. The building direction was shown in Figure 1 (b). After PBF-LS, the specimens were annealed at 473 K for 4.5 hours to release residual stress and cooled in air. In order to avoid crack initiation at a corner of as-built specimen, the corner was rounded by a rubber whetstone of #180 (Tact Polisher Disk T1 #180, Tact Corporation, Kuwana, Japan) and a disc paper #400 (GP100DX-400, Trusco Nakayama Corporation, Tokyo, Japan), as same as previous report [9]. In order to investigate LCP intensity, arc height of stainless-steel plate was measured considering Society of Automotive Engineers SAE standard J442 [70] and J443 [71]. The used stainless-steel was Japanese Industrial Standard JIS SUS304 and the size was 20 mm × 50 mm, 1.5 mm in thickness. Almen strip of N-gauge was also used.

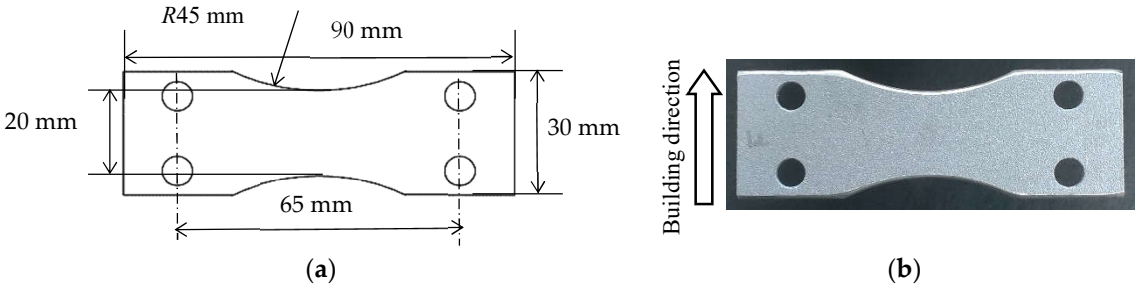

Figure 2. Geometry of plane bending fatigue specimen manufactured by PBF-LS/AlSi10Mg: (**a**) Schematic of specimen (Thickness is 3 mm); (**b**) Photograph of as-built specimen.

2.2. Post-processing

In order to demonstrate improvement of fatigue properties by SLP using a fiber laser and/or a Nd:YAG laser with Q-switch, the specimen was treated by SLP. Figure 3 illustrates a schematic of test section of SLP system. The pulsed laser from the fiber laser or the Nd:YAG laser was irradiated to the specimen, which was placed in water filled chamber by focusing convex lens. The standoff distance in air s_a and in water s_w were defined as shown in Figure 3. The specimen was placed on a stage, which was moved by linear stepping motors in the vertical and horizontal directions. The laser pulse density ρ_L was controlled by the horizontal velocity v_h and the stepwise movement in the vertical direction s_v using the stepping motors. When the repetition frequency of the laser was f_L [Hz], ρ_L was defined by Equation (1).

$$\rho_L = \frac{f_L}{v_h \, s_v} \tag{1}$$

In order to avoid cushion effect at LC-collapse, degassed water was fed into the chamber [72]. A hydrophone (Miniature Hydrophone Type 8103, Brüel & Kjær, HBK Company, Denmark) was set in the chamber to monitor the LC size, as the most important parameter at LCP is LC size. Because the energy of cavitation collapse is proportional to the volume of the cavitation bubble [73], and it was reported that the number of photons was proportional to the maximum diameter of the bubble [74]. Namely, a larger cavitation bubble produces a larger impact during cavitation bubble collapse [75, 76]. The signal was connected to a pre-amplifier (Charge conditioning amplifier 2692, Brüel & Kjær,

 doi:10.20944/preprints202407.2522.v1

HBK Company, Denmark), and recorded by a digital oscilloscope (DPO3054, Tektronix, Inc., Beaverton, OR, USA).

The LC-size was monitored by the developing time t_D of LC obtained from the signal from hydrophone as follows. Regarding Rayleigh [77], the collapse time, t_c, for initial radius of bubble, R_0, to collapse is given by Equation (2).

$$t_c = 0.91468\, R_0 \sqrt{\frac{\rho}{p}} \tag{2}$$

When the values, i.e., pressure p = 0.1013 MPa and density of water ρ = 998 kg/m^3, are substituted into Eq. (2), Eq. (3) is obtained.

$$R_0\,[\mathrm{mm}] = 0.0111\, t_c\,[\mu\mathrm{s}] \tag{3}$$

Regarding previous report [72], when t_D was defined by the time from LA to LC-collapse, d_{max} [mm] was proportional to t_D [μs] and the relation was described as Eq. (4).

$$d_{max}[\mathrm{mm}] = k\, t_D\,[\mu\mathrm{s}] \tag{4}$$

Here k was proportional constant, and it was 0.0103 in the previous report, and it is reasonable by comparing with 0.0111 of Eq. (3), Thus, d_{max} of LC was monitored by t_D.

The aspect of LA and LC was observed by using a high-speed video camera (VW9000, Keyence Corporation, Osaka, Japan). The pixels of full frame size was 640 pixels × 640 pixels, and the maximum frame rate at full frame was 4,000 frame per second. The maximum frame rate was 230,000 frame per second and the frame size was 160 pixels × 32 pixels.

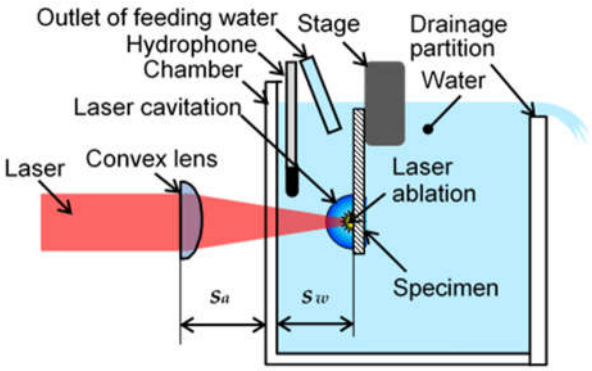

Figure 3. Schematics of test section of submerged laser peening (SLP) system and definition of standoff distance in air s_a and water s_w. .

Figure 4 shows a diagonal view of SLP system using a fiber laser (High power laser system JL-SP0272, Japan Laser Corporation, Tokyo, Japan). The maximum power was 500 W at CW mode, the wave length was 1080 ± 2 nm, the maximum repetition frequency was 50 kHz, the working minimum pulse width was 20 μs, and the maximum divergence was 140 mrad. In Figure 4, the laser beam passage was drawn by a semi-transparent red line. Due to divergence of the fiber laser, a convex lens whose focus distance was 50 mm was placed near the laser head of the fiber laser. The laser beam was reflected by mirrors and then focused by the other convex lens, whose focus distance was 50 mm.

 doi:10.20944/preprints202407.2522.v1

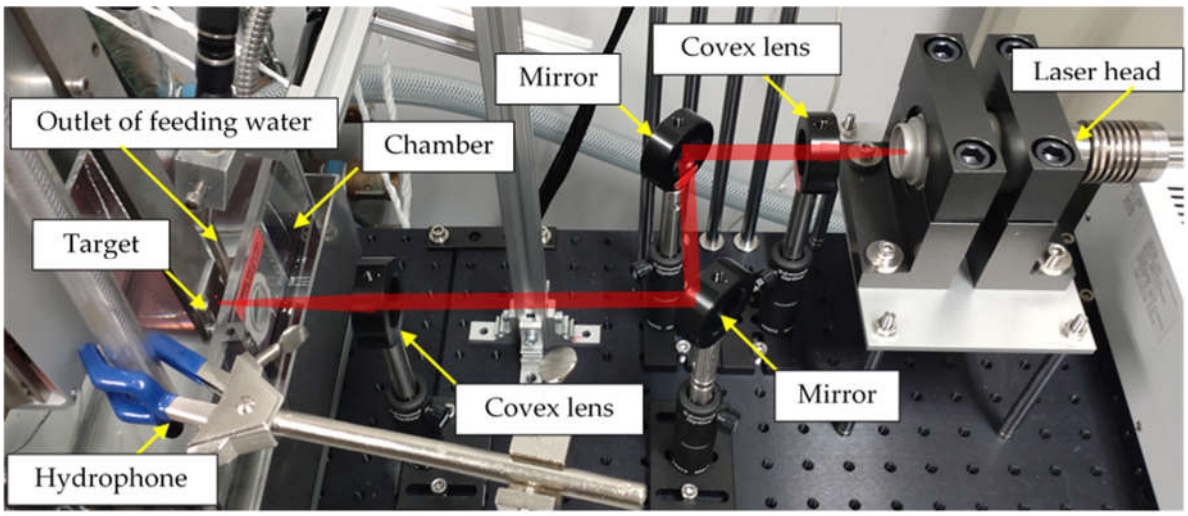

Figure 4. Diagonal view of submerged laser peening (SLP) system using a fiber laser.

Figure 5 reveals a diagonal view of SLP system using a Nd:YAG laser (SureliteTM SL I-10, Continuum®, Amplitude Laser Inc., San Jose, CA, USA). Although the used laser Nd:YAG laser can generate both 532 nm and 1064nm, the used wavelength was 1064 nm considering the previous report [72]. The pulse width, the repetition frequency, the energy, the divergence were 6 ns, 10 Hz, 0.33 J, 0.5 mrad respectively. The laser beam also indicated by the semi-transparent red line in Figure 5. The laser beam was reflected by the mirrors, and expanded by a concave lens whose focus distance was 100 mm, and made parallel beam by a convex lens, then focused by a convex lens to avoid the damage of the chamber.

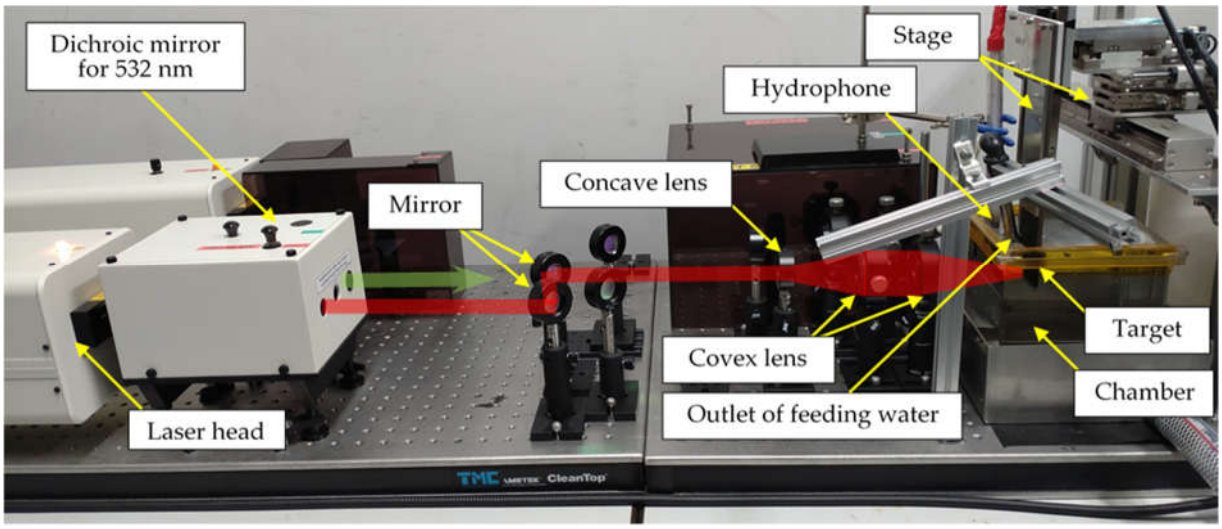

Figure 5. Diagonal view of submerged laser peening system (SLP) using a Nd:YAG laser.

2.3. Fatigue Test and Measurement of Surface Chractersitics

Figure 6 illustrates schematics of plane bending fatigue test machines of (a) moment-controlled type (Advanced PBF, Tokyo Koki Testing Machine Co., Ltd., Sagamihara, Japan) and (b) displacement-controlled type (PBF-30, Tokyo Koki Testing Machine Co., Ltd., Sagamihara, Japan). The moment-controlled type was used to evaluate fatigue life at constant maximum amplitude of applied stress σ_a, as a bending stiffness of the specimen was slightly changed by the post-processing. In order to obtain fatigue strength, the displacement-controlled type was used, as the maximum working frequency was 25 Hz for of the displacement-controlled type and 2 Hz for the moment-controlled type. At both type, stress ratio R was set as −1 for all fatigue test. The applied stress σ_a at

 doi:10.20944/preprints202407.2522.v1

the test was calculated from the bending moment M, the width of the specimen b (i.e., 20 mm), and the thickness δ measured by a micrometer, with an accuracy of 0.001 mm, as shown in Eq. (5).

$$\sigma_a = \frac{6\,M}{b\,\delta^2} \tag{5}$$

At the moment-controlled type, the misalignment of a specimen resulting from the PBF-LS and the post-processing was corrected by the angle of the servomotor, which controlled the angle instantaneously by measuring the moment. Both the torsion angle and torque were monitored and recorded during the fatigue test; a specimen was considered to fail once the torsion angle reached +10° or −10°.

At the displacement-controlled type, the misalignment was corrected by the initial position of the motor. The applied bending moment was monitored by a load cell, and when the bending moment became about 20% of applied bending moment, it was distinguished as failure. The fatigue strength was calculated by using Little's method [78].

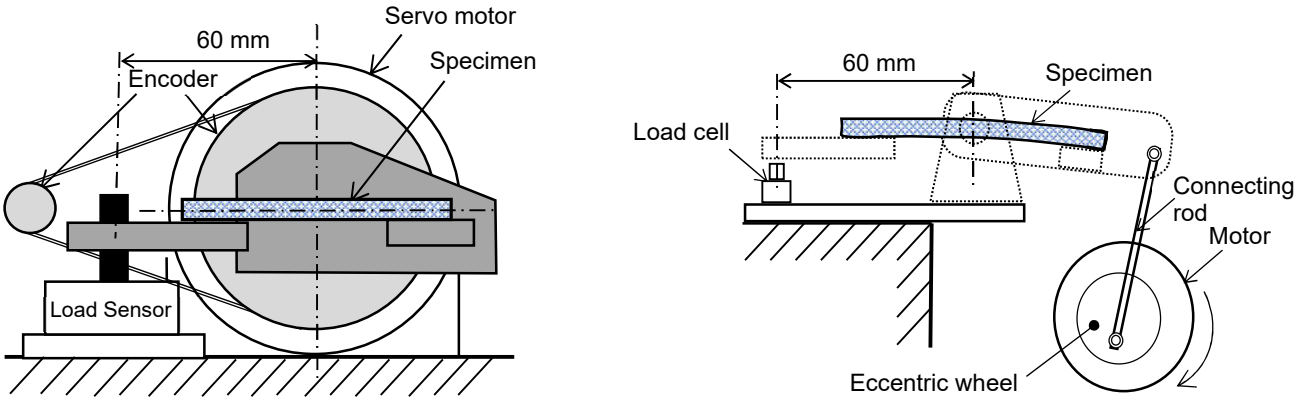

(**a**) (**b**)

Figure 6. Schematics of plane bending fatigue test machines: (**a**) Moment-controlled type; (**b**) Displacement-controlled type.

In order to investigate effect of the post-processing on residual stress, the residual stress σ_R on the surface was evaluated by 2D method [79] using an X-ray diffraction system with a two-dimensional (2D) position sensitive proportional counter (PSPC) (D8 Discover, Bruker Japan K. K., Tokyo, Japan). The used X-ray was Cu-Kα rays (wavelength: 0.1540 Å) operated at 40 kV and 40 mA. The used lattice plane ($h\ k\ l$) was Si (5 3 3) plane, and the diffraction angle without strain was 136.9 degrees. The diffracted X-rays were collected by scanning the specimen surface over an 8 mm × 8 mm area, using a 0.8 mm diameter collimator. The 24 diffraction rings from the specimen at various specimen angle ϕ and incident angle of X-ray ψ were detected (see Figure 7) and the exposure time per frame at each single position was 1 min. Note that the initial position of ω was set at 116°, and it moved to 108° during 1 min to obtain better Debye ring. The residual stress was calculated by using the relevant software (Leptos version 7.9, Bruker Japan K. K., Tokyo, Japan). The used Young's modulus and Poisson's ratio were 167.2 GPa and 0.221, respectively. The analyzed area of the obtained X-ray diffraction as the range of the diffraction angle (2θ = 134° – 140°), and the analyzed area of the Debye ring direction (χ) is in the range of χ = 65° – 115°. The details of 2D method were shown in the reference [79]. As mentioned above, the bending stress was applied in the longitudinal direction of the specimen, and the residual stress in the longitudinal direction of the specimen, i.e., σ_y in Figure 7, are discussed in the present paper.

Preprints.org (www.preprints.org) | NOT PEER-REVIEWED | Posted: 31 July 2024 doi:10.20944/preprints202407.2522.v1

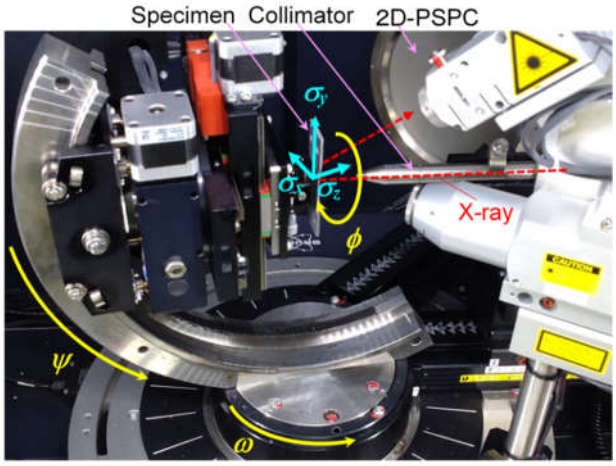

Figure 7. Diagonal view of submerged laser peening system using a Nd:YAG laser.

In order to make clear the effect of surface characteristics on the fatigue properties, surface roughness and hardness were also measured. The arithmetic mean roughness *Ra* was measured by a stylus-type profilometer (Surfcom Touch 50, Tokyo Seimitsu Co., Ltd., Hachioji, Japan) with a cutoff length of 8 mm and a measuring length of 40 mm. The *Ra* was measured in accordance with International Organization for Standardization ISO 21920 [80]. As the surfaces of the specimens were very rough, the surface hardness was measured using a Rockwell superficial hardness tester (ATK-F1000, Akashi Corporation, Tokyo, Japan). For the Rockwell superficial hardness test, a 120° diamond circular cone indenter was used. The initial load was 3 kgf (29 N), and the applied load was 15 kgf (147 N). The hardness was measured seven times in each case, and the average value and standard deviation were obtained from all the values excluding the highest and lowest values. The surface of specimen was observed by a digital microscope (VHX-2000, Keyence Corporation, Osaka, Japan) and a scanning electron microscope (SEM) (JCM-7000, JEOL Ltd., Akishima, Japan).

3. Results

3.1. Laser Ablation (LA) and Laser Cavitation (LC) Generated by a Nd:YAG Laser and a Fiber Laser

In order to reveal a typical aspect of SLP, i.e., LA and LC, aspect of the surface irradiated by the Nd:YAG laser observed by the high-speed video camera was shown in Figure 8 (a). Figure 8 (b) shows a signal detected by the hydrophone, which was recoded simultaneously with the high-speed video camera. At t_L = 0 ms, LA was observed in Figure 8 (a) and peaks were observed in Figure 8 (b). As shown in Figure 8 (a), a hemispherical bubble, i.e., LC, was developed and it had a maximum diameter d_{max} at t_L = 0.53 ms, and shrunk, then collapsed at t_L = 1.05 ms. The d_{max} was 11.2 mm, and t_D was 1,050 μs. Thus, k in Eq. (4) was 0.0107 which was 104% of 0.0103 [72] and 96% of 0.0111 of Eq. (3). As shown in Figure 8 (b), the peaks were observed at t_L = 1.05 ms. The peak – peak at t_L = 1.05 ms was about 180 kPa and it was 12.5% larger than that of LA. As shown in Figure 8 (a), LC was developed again and it was secondly collapsed at t_L = 1.67 ms.

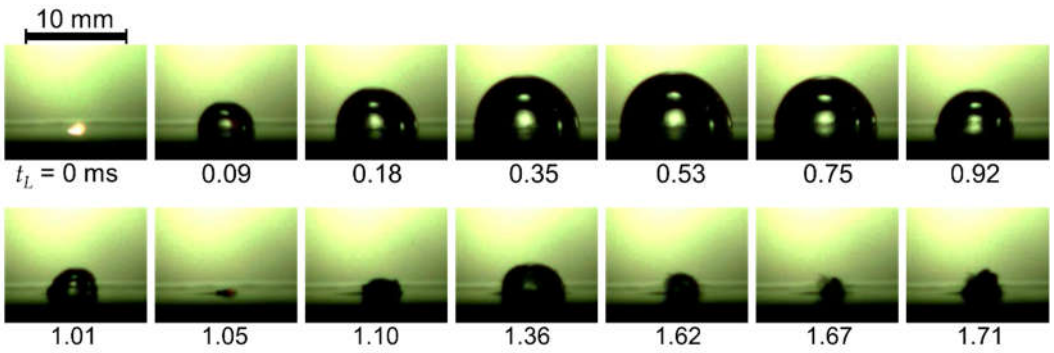

 doi:10.20944/preprints202407.2522.v1

(**a**)

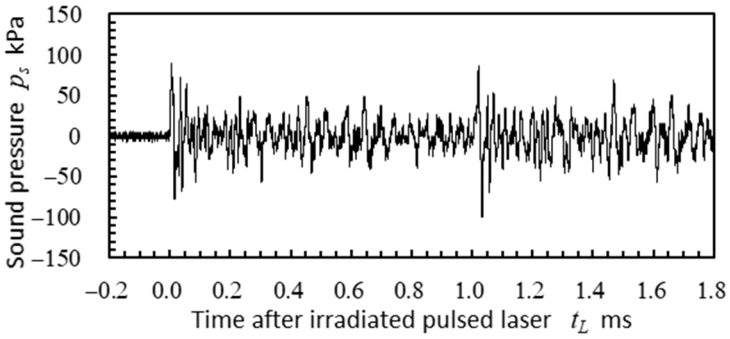

(**b**)

Figure 8. Aspect of laser ablation (LA) and laser cavitation (LC) and sound pressure changing with time after irradiated pulsed laser t_L induced by Nd:YAG laser of wave length λ = 1064 nm and pulse width t_w = 6 ns: (**a**) Aspect of LA and LC; (**b**) Sound pressure p_s.

In order to investigate the possibility of SLP by using the fiber laser, Figure 9 shows the aspect and the noise generated by the fiber laser at t_w = 20 μs and 300 μs. As s_a = 55 mm and s_w = 8 mm were chosen, the noise could not be recorded with the video simultaneously due to the size of the hydrophone, in order to avoid the hydrophone blocking the light. Namely, the video and the noise were recorded separately. As shown in Figure 9 (a) and (b), LA was observed at t_L = 0 ms, and LC was generated after LA, it was developed then collapsed. As shown in Figure 9 (a), at t_w = 20 μs, the 1st collapse of LC was t_L = 0.25 ms and 2nd collapse was at t_L = 0.41 ms. As shown in Figure 9 (b), the amplitude of 1st collapse of LC was about 3 times bigger than that of LA. Namely, SLP using the fiber laser produced LC-collapse impact, which was bigger than that of LA.

In the case of t_w = 300 μs, the 1st collapse of LC was t_L = 0.33 ms and 2nd collapse was at t_L = 0.56 ms, as shown in Figure 9 (c). When the noise was concerned, the amplitude had a peak at t_L = 0 ms and $t_L \approx 0.5$ ms. As mentioned previously, the video and the noise were not recorded simultaneously to avoid the hydrophone blocking the light. From the video and the noise, the amplitude of the noise did not have a peak at the 1st collapse of LC, as the heat of the fiber laser was poured into LC for 0.3 ms, as t_w = 300 μs was nearly equal to the time of the 1st collapse.

When d_{max} of t_w = 20 μs and t_w = 300 μs was compared, it was 2.2 mm for t_w = 20 μs and 2.8 mm for t_w = 300 μs. The maximum amplitude of the noise was about 5 kPa for t_w = 20 μs and 0.9 kPa for t_w = 300 μs. Namely, the LC-collapse impact of t_w = 20 μs was 5.5 times larger than that of t_w = 300 μs, whereas d_{max} of t_w = 300 μs was 1.3 times larger than that of t_w = 20 μs. This result shows that larger LC of t_w = 300 μs generated weaker noise than smaller LC of t_w = 20 μs. It might be caused by cushion effect [72] due to too much heat of the pulsed laser energy at t_w = 300 μs. When k in Eq. (4) was calculated, it was 0.0088 for t_w = 20 μs and 0.0085 for t_w = 300 μs. Namely, k was smaller than that of the Nd:YAG laser. This means that collapsing of LC induced by the fiber laser was slower than that of Nd:YAG laser. And also, LC at t_w = 300 μs was slower than that of t_w = 20 μs. This suggested that LC induced by the longer t_w had a larger cushion effect, and it produced weaker impact.

Regarding previous study, LCP intensity was nearly proportional to the volume of LC considering the threshold of the target material, and it was also proportional to square of the pressure amplitude [72]. When it was assumed that LCP intensity of the fiber laser and the Nd:YAG laser was proportional to the volume of LC, LCP intensity of a single impact by the Nd:YAG laser, whose d_{max} was 11.2 mm, was 132 times larger than that of the fiber laser of t_w = 20 μs, whose d_{max} was 2.2 mm. In the case of the noise, the maximum amplitude of the Nd:YAG laser was about 80 kPa and that of the fiber laser of t_w = 20 μs was about 5 kPa, then $(80/5)^2$ was 256. Namely, at the present condition, LCP by the Nd:YAG laser was 136 – 256 times stronger than LCP by the fiber laser. As mentioned above, as the maximum repetition frequency of the fiber laser was 50 kHz, which was 5,000 times larger than that of the Nd:YAG laser, the fiber laser might be used for LCP, if the parameters such as the t_w, s_w, s_a, local distance of convex lens etc. were optimized. However, SLP by the fiber laser was examined to be used for as LT in the present paper.

 doi:10.20944/preprints202407.2522.v1

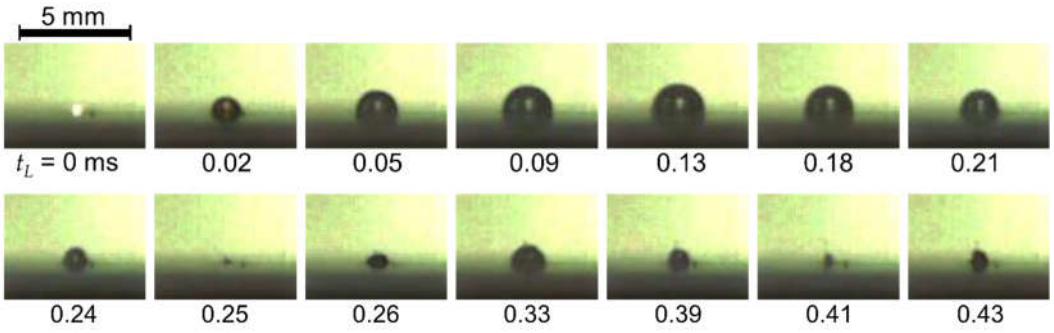

(**a**) t_w = 20 μs

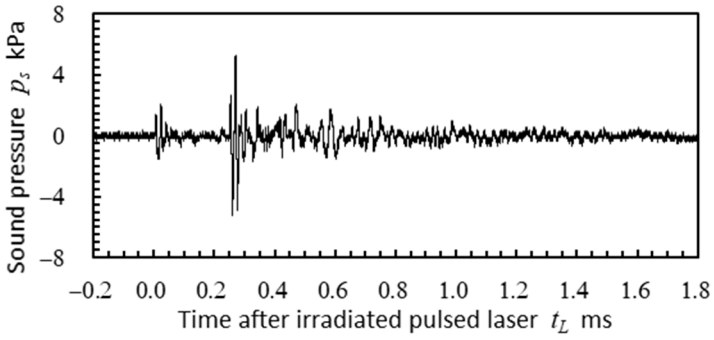

(**b**) t_w = 20 μs

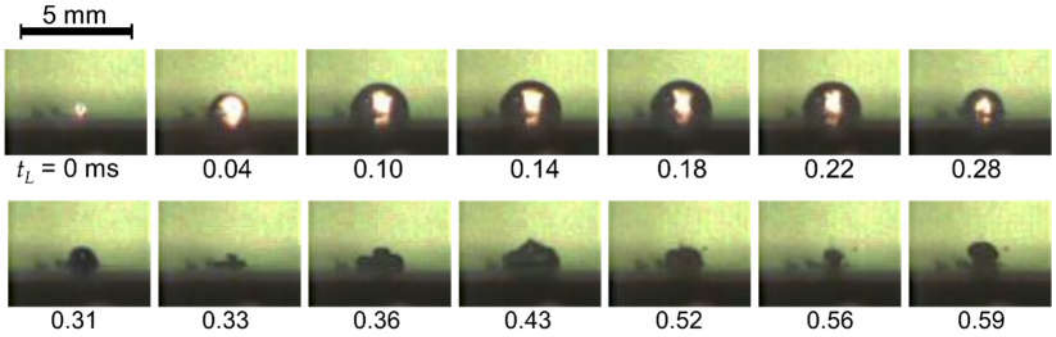

(**c**) t_w = 300 μs

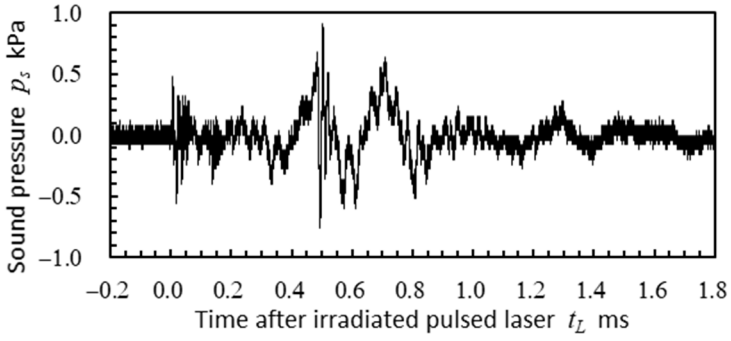

(**d**) t_w = 300 μs

Figure 9. Aspect of laser ablation (LA) and laser cavitation (LC) and sound pressure changing with time after irradiated pulsed laser t_L induced by fiber laser of wave length λ = 1080 nm at pulse width t_w = 20 μs and 300 μs: (**a**) Aspect of LA and LC at t_w = 20 μs; (**b**) Sound pressure p_s at t_w = 20 μs; (**c**) Aspect of LA and LC at t_w = 300 μs; (**d**) Sound pressure p_s at t_w = 300 μs.

3.2. Determination of Submerged Laser Peening (SLP) Conditions Using a Fiber Laser

As this is the first report about SLP using the fiber laser, effect of parameters such as t_w and s_w on SLP were investigated. Figures 10 and 11 reveal the arc height h changing with t_w and s_w,

 doi:10.20944/preprints202407.2522.v1

respectively. At both cases, s_a was chosen as 55 mm. In order to obtain Figure 10, s_w was 8 mm, and the repetition frequency was chosen as laser energy per unit time should be equivalent. At Figure 11, t_w was chosen as 300 μs and the repetition frequency 300 Hz, ρ_L = 50 pulse/mm^2, considering the result of Figure 10. At the present conditions, all specimens were deformed with treated surface concave. At conventional SLP using the Nd:YAG laser, the specimens were deformed with treated surface convex, as the treated surface was plastically elongated. The present result of deformation of the treated surface into a concave surface clearly indicates that the treated surface was shrinking. As mentioned in Figure 1, SLP is classified to two stage, i.e., LA-stage and LC-collapse-stage. At LA-stage, the surface is melted by the heat energy of the pulsed laser. Although LC-collapse noise produced by the fiber laser was detected as shown in Figure 9 (b), SLP by the fiber laser was governed by LA-stage rather than LC-collapse-stage. Then, as mentioned in Figure 1, SLP governed by LA-stage was classified into laser treatment (LT) in the present paper. Thus, SLP by the fiber laser will henceforth be referred to as LT. Therefore, the condition of SLP by the fiber laser was chosen as the condition that deformed the most concave surface was selected, i.e., t_w = 300 μs and s_w = 8 mm.

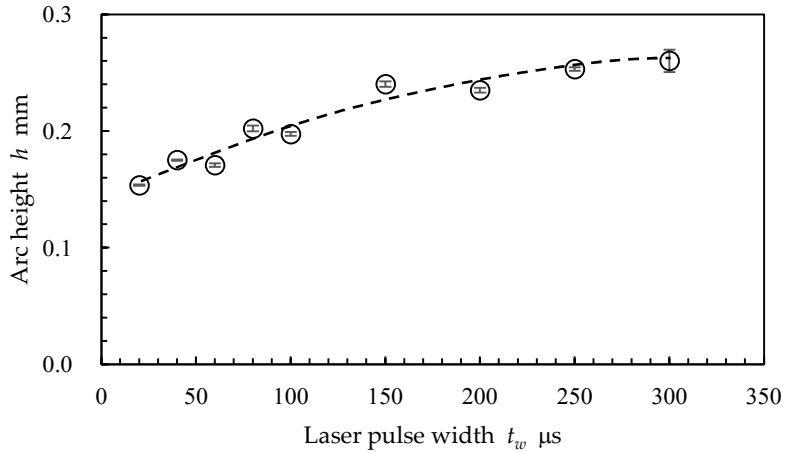

Figure 10. Effect of pulse width t_w on laser treatment (LT) using fiber laser.

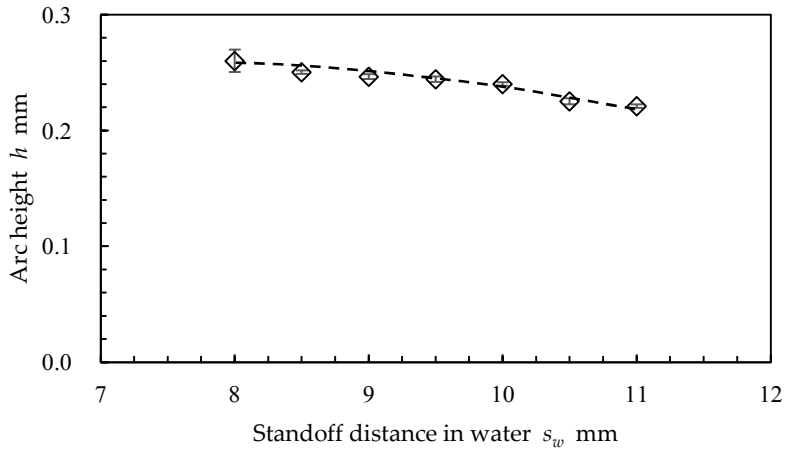

Figure 11. Effect of standoff distance in water s_w on laser treatment (LT) using fiber laser.

3.3. Aspect of Surface Treated by Post-Processing

Aspect of treated surfaces observed by the digital microscope and SEM were shown in Figs. 12 and 13, respectively. Each Figs. 12 and 13 reveals (a) As-built, (b) Laser Treatment (LT; SLP by the fiber laser), (c) Blasting (B), (d) Laser Cavitation Peening (LCP; SLP by the Nd:YAG laser), (e) Blasting + Laser Treatment, (f) Laser Treatment + Laser Cavitation Peening, (g) Blasting + Laser Cavitation Peening and (h) Blasting + Laser Treatment + Laser Cavitation Peening. At laser treatment (LT), i.e.,

 doi:10.20944/preprints202407.2522.v1

SLP by the fiber laser, the repletion frequency, the pulse width t_w and the pulse density ρ_L were 300 Hz, 300 μs and 50 pulse/mm^2, respectively. The blasting (B) was carried out at air pressure 0.7 MPa using garnet #150, considering previous report [11]. At laser cavitation peening (LCP), i.e., SLP by the Nd:YAG laser, the repetition frequency was 10 Hz and ρ_L was 4 pulse/mm^2, considering previous report [9, 50].

On the as-built surface, partially melted particles were observed as shown in Figure 12 (a) and Figure 13 (a). The deep valleys, which lied perpendicularly to building direction, were also observed, and the bottom of the valley was very sharp as shown in Figure 13 (a). These surface defects might become crack sources during the fatigue.

When the as-built surface was treated by LT, many columnar structures were observed as shown in Figure 12 (b) and Figure 13 (b). The pulsed laser ablated Al-phase, then Si-phase, which were shown as columnar structures, was remained.

After blasting (B) of as-built surface, the sharp edges were roughened by the blasting as shown in Figure 13 (c). These roughed surfaces reduced the reflection of the pulsed laser, then the LA-effect was increased. Namely, blasting enhanced the effect of LT and/or LCP.

In the case of LCP, the fine microstructures were observed as shown in Figure 12 (d) and Figure 13 (d). These structures were produced by ns-seconds laser pulses.

When the surface was treated by LT after blasting, the melted structures, which were larger than that of LCP were observed as shown in Figure 12 (e) and Figure 13 (e). At the present condition, the power was 45 W for LT, i.e., SLP by the fiber laser, and 3 W for LCP, i.e., SLP by the Nd:YAG laser. Namely, larger laser power melted the surface and it produced large structures.

After LT and LCP, the microstructures, whose size was in between surface treated by LT and LCP, were observed as shown in Figure 12 (f) and Figure 13 (f). The surface was partially melted by LT, and the surface became similar aspect of Figure 12 (e) and Figure 13 (e), then ablated by LCP, i.e., short pulsed laser of 6 ns in pulse width.

When the surface was treated by LCP after blasting (see Figure 12 (g) and Figure 13 (g)), the microstructures seems to be slightly larger than that of LCP only. As mentioned above, blasted surface was more likely to absorb laser energy, then the surface was considered to be more melted.

As shown in Figure 12 (h) and Figure 13 (h), at B + LT + LCP, the surface was melted by the fiber laser and then ablated by the Nd:YAG laser. The microstructures were similar to that of Figure 12 (g) and Figure 13 (g), and the size of microstructures were slightly larger than that of B + LCP, as the surface was melted by LT.

 doi:10.20944/preprints202407.2522.v1

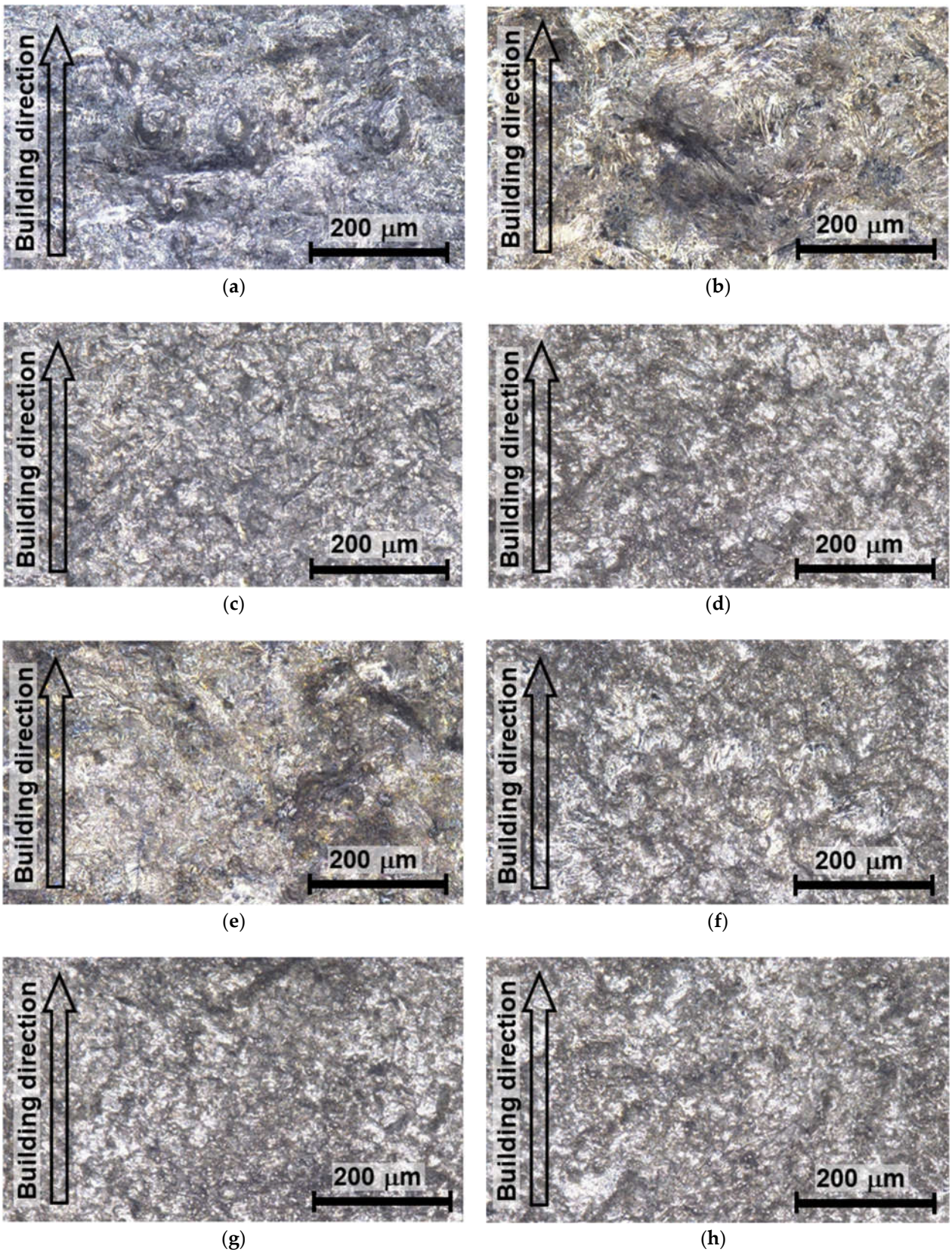

Figure 12. Aspect of specimen observed by digital microscope: (**a**) As-built; (**b**) Laser treatment (LT; SLP by fiber laser); (**c**) Blasting (B); (**d**) Laser cavitation peening (LCP; SLP by Nd:YAG laser); (**e**) B + LT; (**f**) LT + LCP; (**g**) B + LCP; (**h**) B + LT + LCP.

 doi:10.20944/preprints202407.2522.v1

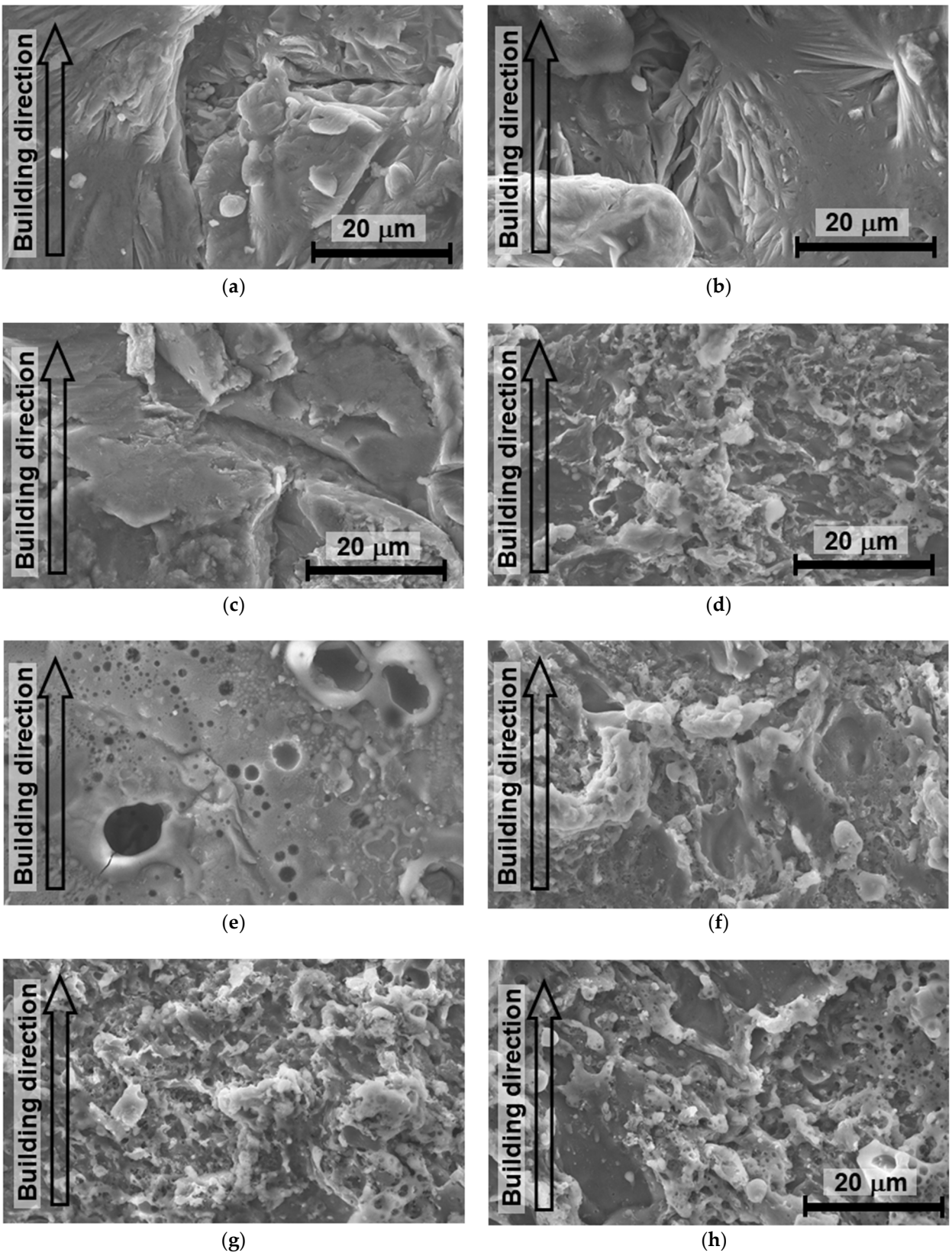

Figure 13. Aspect of specimen observed by scanning electron microscope (SEM): (**a**) As-built; (**b**) Laser treatment (LT; SLP by fiber laser); (**c**) Blasting (B); (**d**) Laser cavitation peening (LCP; SLP by Nd:YAG laser); (**e**) B + LT; (**f**) LT + LCP; (**g**) B + LCP; (**h**) B + LT + LCP.

3.4. Effects of Post-Processing on Fatgiue Properties and Surface Properties

 doi:10.20944/preprints202407.2522.v1

In order to reveal the effects of post-processing, i.e., blasting (B), laser treatment (LT), laser cavitation peening (LCP) and the combined processes of these post-processing, Figure 14 reveals (a) fatigue life at σ_a = 110 MPa evaluated by the moment-control type plane bending fatigue tester, (b) surface roughness *Ra*, (c) residual stress σ_R, (d) Rockwell hardness H_{R15T} and (e) full width at half maximum of X-ray diffraction pattern *FWHM*. The post-processing conditions to obtain Figure 14 were same condition of Figs. 12 and 13.

In the case of fatigue life at σ_a = 110 MPa, three time of as-built was evaluated, and it was 73,525, 73,904 and 84,822. Then, average value was 77,417 and the standard deviation was 6,416, which was 8.28 % of average value. In the case of post-processing, the fatigue life was tested at once, and the error bars in Figure 14 (a) was 8.28 % of each average value.

At LT, as shown in Figure 14 (a), the fatigue life was shortened by LT, whereas the surface was smoothed by LT (see Figure 14 (b)). The reason would be that the residual stress after LT was tension as shown in Figure 14 (c). As shown in Figure 14 (e), *FWHM* of LT was increased drastically, and the surface was melted by LT (see Figure 12 (b) and Figure 13 (b)). Thus, LT melted the as-built surface and quenched the surface because of SLP.

In the case of blasting (B), B reduced the surface roughness (see Figure 14 (b)), introducing the compressive residual stress (see Figure 14 (c)). These effects improved the fatigue life.

At LCP, the surface was smoothed as same as B (see Figure 14 (b)), and the compressive residual stress was introduced (see Figure 14 (c)). Thus, the fatigue life was improved by LCP as shown in Figure 14 (a).

In the case of combined process with B, such as B + LT and B + LCP, effect of LT and LCP was enhanced by B, as blasted surface absorbed the pulsed laser energy by decreasing the reflection. For example, the surface roughness of B + LT or B +LCP was smoother than that of LT or LCP (see Figure 14 (b)). The residual stress of B + LT was more tension than that of LT, and the residual stress of B + LCP was more compression than that of LCP, as shown in Figure 14 (d). In the case of combined process of LT + LCP, the introduced residual stress was −480 ± 24 MPa, which was more compression than LCP only (−135 ± 20 MPa), whereas LT introduced tensile residual stress (412 ± 31 MPa).

As shown in Figure 14 (d), the Rockwell hardness H_{R15T} was increased by LT + LCP and B + LT + LCP. It was also slightly increased by LT and B. On the other hand, H_{R15T} was decreased by LCP and B + LCP. As the surface roughness of as-built surface was very rough, the scatter band of all cases were large. Namely, it was very difficult to evaluate hardness on the surface of as-built PBF-LS/AlSi10Mg.

As shown in Figure 14 (a), in the case of the fatigue life at σ_a = 110 MPa, B + LT + LCP was best, LT + LCP was 2nd, B + LCP was 3rd, and B and LCP were 4th. Thus, B + LT + LCP was chosen as the post-processing for the evaluation of the fatigue strength. As previous report, LCP was best comparing with SP and CP by jet, the fatigue strength of LCP was also examined.

Preprints.org (www.preprints.org) | NOT PEER-REVIEWED | Posted: 31 July 2024 doi:10.20944/preprints202407.2522.v1

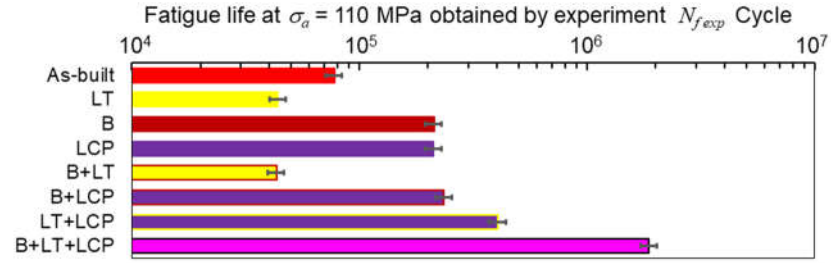

(**a**)

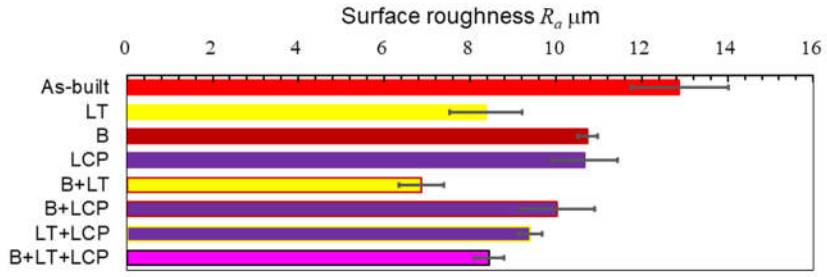

(**b**)

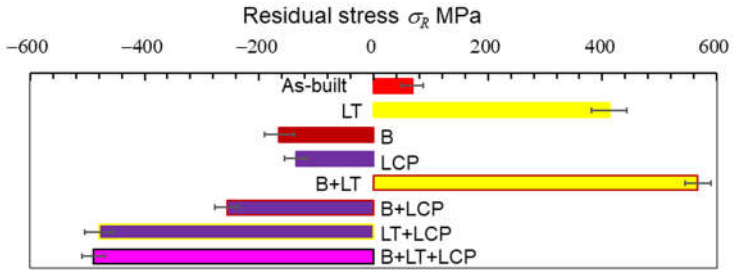

(**c**)

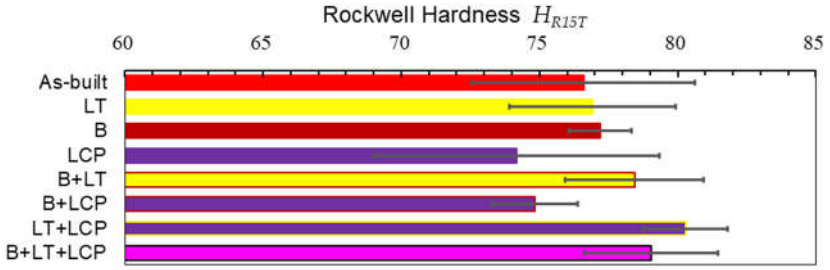

(**d**)

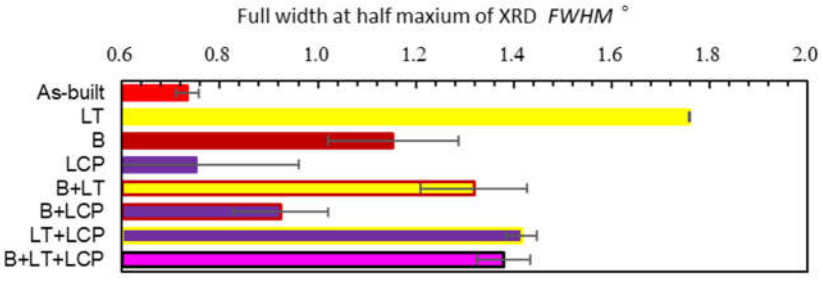

(**e**)

Figure 14. Mechanical properties of as-built, laser treatment (LT), blasting (B), laser cavitation peening (LCP), B+LT, B+LCP, LT+LCP and B+LT+LCP: (**a**) Fatigue life at σ_a = 110 MPa; (**b**) Surface roughness R_a; (**c**) Residual stress σ_R; (**d**) Rockwell hardness H_{R15T}; (**e**) Full width at half maximum of X-ray diffraction pattern *FWHM*.

 doi:10.20944/preprints202407.2522.v1

In order to reveal the improvement of the fatigue strength of as-built PBF-LS/AlSi10Mg by post-processing, Figure 15 illustrates S-N curve for as-built, LCP and B + LT + LCP obtained by the displacement-controlled type plane bending fatigue tester. The post-processing conditions which used to obtain Figure 15 were same condition of Figs. 12 – 14. Namely, the blasting (B) was carried out at air pressure 0.7 MPa using garnet #150 [11]. At LT by the fiber laser, the repletion frequency, the pulse width t_w and the pulse density ρ_L were 300 Hz, 300 μs and 50 pulse/mm², respectively. LCP by the Nd:YAG laser was carried out at the repetition frequency 10 Hz and ρ_L = 4 pulse/mm² [9, 50]. To compare the fatigue properties of as-built PBF-LS/AlSi10Mg with cast AlSi10Mg, S-N curve of smooth specimens evaluated by the cyclic bending multiple fatigue tester at R = –1 [81] was illustrated in Figure 15. As shown in Figure 15, the fatigue properties of as-built PBF-LS/AlSi10Mg were weak comparing with cast AlSi10Mg. When the fatigue strength at $N = 10^7$ was calculated by Little's method [78], it was 54 ± 9 MPa for as-built, 85 ± 10 MPa for LCP and 103 ± 12 MPa for B + LT + LCP. Namely, B + LT + LCP enhanced the fatigue strength of PBF-LS/AlSi10Mg by 1.91 times comparing with as-built one, and it was larger than that of LCP only.

In order to compare the present result with the references [16, 24, 26], Table 1 shows the fatigue strength of as-built and post-processing PBF-LS/AlSi10Mg. The improvement ratio comparing with as-built and post-processing of B + LT + LCP was better than reported results except notched one, as the fatigue strength of notched as-built specimen was quite weak. Namely, the proposed post-processing is worthwhile to use for practical applications.

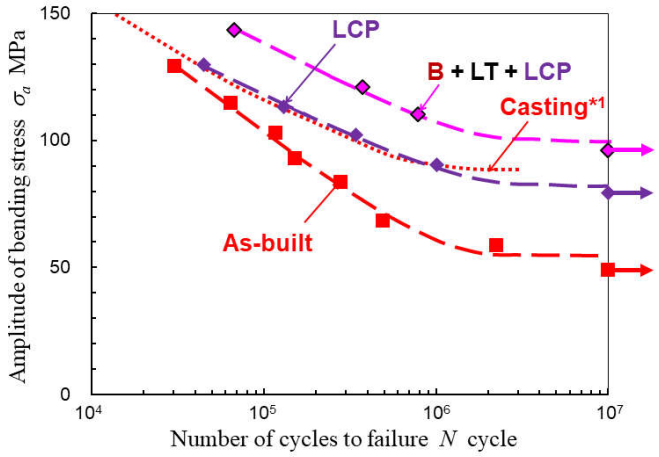

Figure 15. Improvement of fatigue strength of as-built PBF-LS/AlSi10Mg by blasting (B), laser treatment (LT) and laser cavitation peening (LCP).

Table 1. Fatigue strength of as-built AlSi10Mg.

Specimen	As-built	Post-processing		Improvement ratio
Fatigue strength at 10^7 [present] (Plane bending, R = –1)	54 MPa	LCP	85 MPa	57 %
		B+LT+LCP	103 MPa	91 %
Fatigue strength at 3×10^6 [16] (Rotating bending, R = –1 with notch)	10 MPa	SP1	72 MPa	(720 %)
		SP2	92 MPa	(920 %)
Fatigue strength at 10^6 [26] (Plane bending, R = 0)	56 MPa	LP	90 MPa	61 %
		SP	89 MPa	59 %
Fatigue strength at 10^7 [26] (Plane bending, R = 0)	51 MPa	LP	90 MPa	76 %
		SP	81 MPa	59 %
Fatigue strength at 10^7 [24] (Rotating bending, R = –1)	75 MPa	Polished	100 MPa	33 %
		Polished + SP	110 MPa	47 %

3.5. Estimation of Improved Fatgiue Life by Post-Processing Using Surface Roughness, Residual Stress and Hardness

In order to find out key parameters in improvement of fatigue properties of PBF-LS/AlSi10Mg by post-processing, an estimation method of the improved fatigue life was discussed. Because the

 doi:10.20944/preprints202407.2522.v1

fatigue properties should be estimated from the key parameters, if the key parameters on the improvement were identified.

Considering the previous reports [12][14], experimental correlation formulas, which were described by Eqs. (6) and (7), were proposed to estimate improved fatigue life by using the surface roughness, residual stress and hardness. Here, $N_{f\,est}$ and $N_{f\,AB}$ are estimated number of cycles and number of cycles of as-built. The c_S, c_R and c_H are sensitivity constants representing the effects of the surface roughness, residual stress and hardness, respectively. In Eqs. (6) and (7), the effects of the surface roughness, residual stress and hardness were normalized by the surface roughness Ra_{AB}, the residual stress $\sigma_{R\,AB}$ considering applied stress σ_a, and the hardness $H_{R15T\,AB}$ of the as-built specimen, respectively.

$$N_{f\,est} = N_{f\,AB}\left\{1 + c_S\frac{1}{\frac{R_a}{R_{a\,AB}}} + c_R\left(\frac{\sigma_{R\,AB} - \sigma_R}{\sigma_a}\right)\right\} \quad (6)$$

$$N_{f\,est} = N_{f\,AB}\left\{1 + c_S\frac{1}{\frac{R_a}{R_{aAB}}} + c_R\left(\frac{\sigma_{R\,AB} - \sigma_R}{\sigma_a}\right) + c_H\frac{H_{R15T}}{H_{R15TAB}}\right\} \quad (7)$$

The c_S, c_R and c_H were calculated by a least square method using measured values in Table 2. The obtained constants, i.e., c_S, c_R and c_H are shown in Table 3. The relation between $N_{f\,exp}$ and $N_{f\,est}$ obtained by Eqs. (6) and (7) are shown in Figure 16 (a) and (b). The obtained slope a_{best} of the relation between $N_{f\,exp}$ and $N_{f\,est}$ is also revealed in Table 3, with its standard deviation σ_s (see Eq. (8)).

$$N_{f\,est} = (a_{best} \pm \sigma_s)\ N_{f\,\exp} \quad (8)$$

In Table 3, correlation coefficient r and determination coefficient D_c are also revealed. Probability of a non-correlation p_{non} of 7 data was calculated from r [82].

Table 2. Measured value of number of cycles to failure, surface roughness, residual stress and hardness.

Post-processing	Number of cycles to failure $N_{f\,exp}$ [cycles]	Arithmetical mean roughness Ra [μm]		Residual stress σ_R [MPa]		Rockwell hardness $H_{R15T\,AB}$	
		Average value	Standard deviation	Average value	Standard deviation	Average value	Standard deviation
As-built	77,417	12.88	1.14	68	19	76.6	4.0
LT	43,862	8.37	0.85	412	31	76.9	3.0
B	211,922	10.74	0.24	–165	26	77.2	1.1
LCP	211,419	10.68	0.77	–135	20	74.2	5.2
B + LT	43,134	6.86	0.52	567	23	78.4	2.5
B + LCP	234,637	10.03	0.88	–256	20	74.8	1.5
LT + LCP	404,759	9.40	0.27	–480	24	80.3	1.5
B + LT + LCP	1,865,502	8.44	0.35	–489	20	79.0	2.4

Table 3. Constants for experimental formula to estimate fatigue life by surface roughness, residual stress and hardness.

	Symbol	Eq. (6)	Eq. (7)
Constant for surface roughness	c_S	0.192	0.181

 doi:10.20944/preprints202407.2522.v1

Constant for residual stress	c_R	0.162	0.160
Constant for hardness	c_H	–	0.023
Slope	a_{best}	1.082	1.075
Standard deviation of slope	σ_s	0.028	0.035
Correlation coefficient	r	0.933	0.936
Determination coefficient	D_c	0.870	0.831
Probability of a non-correlation	p_{non}	0.22%	0.20%

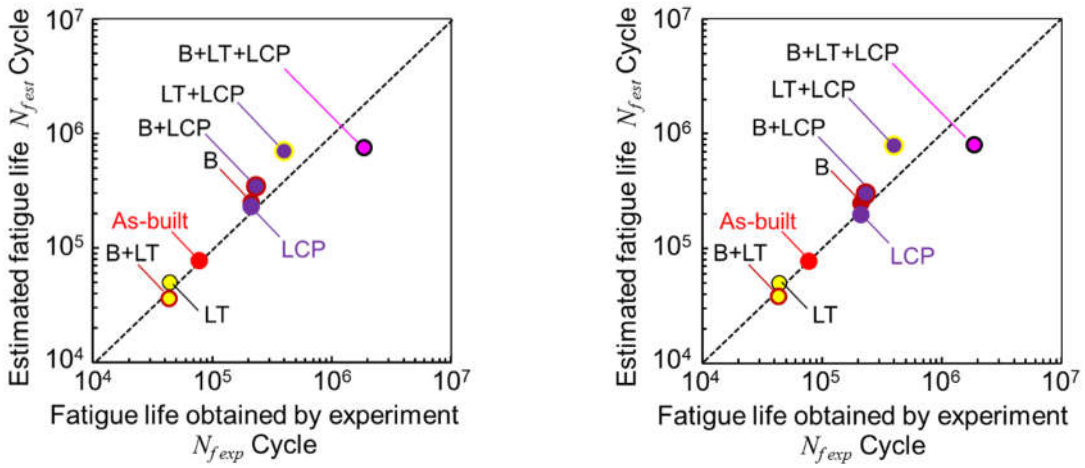

Figure 16. Estimated fatigue life N_{fest} from fatigue life obtained by experiment N_{fexp} at σ_a = 110 MPa using mechanical properties of surface: (**a**) Eq. (6); Surface roughness R_a and residuals stress σ_R; (**b**) Eq. (7); Surface roughness R_a, residuals stress σ_R and Rockwell hardness $H_{R\,15T}$.

As shown in Figure 16 (a) and (b), N_{fest} was proportional to N_{fexp}, and its slope was 1.082 ± 0.028 and 1.075 ± 0.035. When p_{non} is smaller than 1 %, it can be said the relation is highly significant. As shown in Table 3, p_{non} of both Eqs. (6) and (7) is less than 1 %, thus it can be concluded that relation between N_{fexp} and N_{fest} was highly significant. Namely, improved fatigue life by post-processing can be estimated by surface roughness, residual stress and hardness.

When c_s, c_R and c_H in Table 3 were compared, $c_s > c_R >> c_H$ were obtained. This means that the contribution of surface smoothing is more effective than the introduction of compressive residual stress on the improvement of fatigue life by post-processing, and the effect of work hardening is less effective than surface smoothing and introduction of compressive residual stress. As r of Eq. (6) was nearly equal to that of Eq. (7), the improvement of fatigue life of as-built PBF-LS/AlSi10Mg by post-processing can be estimated by surface roughness and residual stress on the surface. Namely, the main factors of the improvement of fatigue properties of as-built PBF-LS/AlSi10Mg by post-processing were the surface roughness and the residual stress on the surface.

4. Conclusions

In order to demonstrate improvement of fatigue properties of AM metals by submerged laser peeing (SLP), powder bed fusion (PBF) using laser sintering (LS) AlSi10Mg, i.e., PBF-LS/AlSi10Mg was treated by SLP using a fiber laser whose maximum repetition frequency was 50 kHz and/or a Nd:YAG laser whose maximum repetition frequency was 10 Hz, and tested by plane bending fatigue tests. In the present paper, to distinguish effect of laser ablation (LA) and laser cavitation (LC) at SLP, post-processing governing by LA and LC were named as laser treatment (LT) and laser cavitation peening (LCP), respectively. The results obtained can be summarized as follows:

 doi:10.20944/preprints202407.2522.v1

1. At SLP using the fiber laser, LC was observed. The amplitude of pressure wave generated by LC collapse was 3 times larger than that of LA. At the present condition, SLP using the fiber laser smoothen the surface of as-built PBF-LS/AlSi10Mg, and the surface residual stress was tensile after SLP using the fiber laser. Thus, SLP using the fiber laser was LT rather than LCP.
2. Blasting (B) roughened the as-built surface of PBF-LS/AlSi10Mg, and enhanced the effect of following LT, as blasted surface absorbed the pulsed laser energy. LT, i.e., SLP by the fiber laser, melted the as-built surface, and quenched the surface, then introduced tensile residual stress. LCP, i.e., SLP by the Nd:YAG laser, introduced compressive residual stress into as-built surface. In the case of the fatigue life at σ_a = 110 MPa, B + LT + LCP was best, LT + LCP was 2nd, B + LCP was 3rd, and B or LCP were 4th.
3. In the case of fatigue strength of PBF-LS/AlSi10Mg at 10^7, B + LT + LCP was 103 ± 12 MPa, LCP was 85 ± 10 MPa, whereas as-built was 54 ± 9 MPa. Namely, B + LT + LCP improved the fatigue strength 1.9 times comparing with the as-built.
4. LT + LCP introduced compressive residual stress (−480 ± 24 MPa) which was larger than that of enhanced LCP only (−135 ± 20 MPa), although LT introduced tensile residual stress (412 ± 31 MPa).
5. The improvement of fatigue strength of as-built PBF-LS/AlSi10Mg can be estimated by surface roughness and the surface residual stress. The work hardening also contributed the improvement of the fatigue strength, however, the contribution of work hardening in improving fatigue strength was relatively small, considering the difficulty in evaluating hardness of as-built PBF-LS/AlSi10Mg due to rough surface.
6. Regarding SLP by the fiber laser, when the pulse width was shorter, the sound pressure of LC collapse became larger. At LC collapse using the larger pulse width, the sound pressure of 1st LC collapse became smaller, and that of 2nd LC collapse became larger, as heat energy was introduced into bubble during 1st shrinking of LC.

Author Contributions: Hitoshi Soyama, conceptualization, experiment, writing—original draft, visualization, project administration, and funding acquisition.

Funding: This research was partly supported by JSPS KAKENHI (grant numbers 22KK0050 23K25988), JST CREST (JPMJCR2335) and Suzuki Foundation (5-i19).

Institutional Review Board Statement: Not applicable.

Informed Consent Statement: Not applicable.

Data Availability Statement: The data presented in this study are available upon request from the author.

Conflicts of Interest: The author declares no conflicts of interest.

Abbreviations

2D	two-dimension
AB	as-built
AM	additive manufacturing
B	blasting
CAD	computer-aided design
CAM	computer-aided manufacturing
CP	cavitation peening
HIP	hot isostatic pressing
ISO	International Organization for Standardization
JIS	Japanese Industrial Standards
LA	laser ablation
LC	laser cavitation
LCP	laser cavitation peening
LP	laser peening
LS	laser sintering

 doi:10.20944/preprints202407.2522.v1

LT	laser treatment
PBF	powder bed fusion
PSPC	position sensitive proportional counter
PVDF	polyvinylidene fluoride
SAE	Society of Automotive Engineers
SLP	submerged laser peening
SP	shot peening
XRD	X-ray diffraction

Symbol

a_{best}	slope
b	width of specimen
c_H	constant for surface hardness
c_R	constant for surface residual stress
c_s	constant for surface roughness
D_c	determination coefficient
d_{max}	maximum diameter of LC
E	Young's modulus
$FWHM$	Full width at half maximum of X-ray diffraction
f_L	repetition frequency of the laser
H_{R15T}	Rockwell hardness
h	arc height
k	proportional constant
M	bending moment
N	number of cycles to failure
$N_{f\,est}$	estimated fatigue life
$N_{f\,exp}$	fatigue life obtained by experiment
p	pressure
p_{non}	probability of a non-correlation
p_s	sound pressure detected by hydrophone
R	stress ratio
R_0	initial radius of bubble
R_a	surface roughness
r	correlation coefficient
s_a	standoff distance in air
s_v	vertical direction
s_w	standoff distance in water
t_c	collapse time of bubble
t_L	time after irradiated pulsed laser
t_D	developing time of LC
t_w	laser pulse width
v_h	horizontal velocity
χ	Debye ring direction
δ	thickness of specimen
ϕ	rotation angle of specimen
θ	diffraction angle
ρ	density of water
ρ_L	laser pulse density
λ	wave length
ν	Poisson ratio
σ_a	applied stress
σ_R	residual stress

σ_s	standard deviation of slope
ψ	incidence angle

References

1. Murr, L.E.; Gaytan, S.M.; Ramirez, D.A.; Martinez, E.; Hernandez, J.; Amato, K.N.; Shindo, P.W.; Medina, F.R.; Wicker, R.B. Metal fabrication by additive manufacturing using laser and electron beam melting technologies. *J. Mater. Sci. Technol.* **2012**, 28, 1-14.
2. Wang, X.J.; Xu, S.Q.; Zhou, S.W.; Xu, W.; Leary, M.; Choong, P.; Qian, M.; Brandt, M.; Xie, Y.M. Topological design and additive manufacturing of porous metals for bone scaffolds and orthopaedic implants: A review. *Biomaterials* **2016**, 83, 127-141.
3. DebRoy, T.; Wei, H.L.; Zuback, J.S.; Mukherjee, T.; Elmer, J.W.; Milewski, J.O.; Beese, A.M.; Wilson-Heid, A.; De, A.; Zhang, W. Additive manufacturing of metallic components - process, structure and properties. *Prog. Mater. Sci.* **2018**, 92, 112-224.
4. You, S.G.; You, S.M.; Kang, S.Y.; Bae, S.Y.; Kim, J.H. Evaluation of the adaptation of complete denture metal bases fabricated with dental CAD-CAM systems: An in vitro study. *J Prosthet Dent* **2021**, 125, 479-485.
5. Wang, P.; Li, X.; Luo, S.; Nai, M.L.S.; Ding, J.; Wei, J. Additively manufactured heterogeneously porous metallic bone with biostructural functions and bone-like mechanical properties. *J. Mater. Sci. Technol.* **2021**, 62, 173-179.
6. Alammar, A.; Kois, J.C.; Revilla-Leon, M.; Att, W. Additive manufacturing technologies: Current status and future perspectives. *J Prosthodont* **2022**, 31, 4-12.
7. Edwards, P.; O'Conner, A.; Ramulu, M. Electron beam additive manufacturing of titanium components: Properties and performance. *J. Manuf. Sci. Eng. Trans. ASME* **2013**, 135, 1-7.
8. Kahlin, M.; Ansell, H.; Moverare, J.J. Fatigue behaviour of notched additive manufactured Ti6Al4V with as-built surfaces. *Int. J. Fatigue* **2017**, 101, 51-60.
9. Soyama, H.; Sanders, D. Use of an abrasive water cavitating jet and peening process to improve the fatigue strength of titanium alloy 6Al-4V manufactured by the electron beam powder bed melting (EBPB) additive manufacturing method *JOM* **2019**, 71, 4311–4318.
10. Kahlin, M.; Ansell, H.; Kerwin, A.; Smith, B.; Moverare, J. Variable amplitude loading of additively manufactured Ti6Al4V subjected to surface post processes. *Int. J. Fatigue* **2021**, 142, 12.
11. Soyama, H., Improvement of fatigue strength of 3D-metal by combined process of blasting and cavitation peening, Proceedings of the 3rd international conference on advanced surface enhancement (INCASE) 2023, **2024**, pp. 23-29, DOI: 10.1007/978-981-99-8643-9_3
12. Soyama, H.; Wong, K.L.; Eakins, D.; Korsunsky, A.M. The effects of submerged laser peening, cavitation peening, and shot peening on the improvement of the torsional fatigue strength of powder bed fused Ti6Al4V produced through laser sintering. *Int. J. Fatigue* **2024**, 185, 108348.
13. Kahlin, M.; Ansell, H.; Basu, D.; Kerwin, A.; Newton, L.; Smith, B.; Moverare, J.J. Improved fatigue strength of additively manufactured ti6al4v by surface post processing. *Int. J. Fatigue* **2020**, 134, 105497.
14. Sanders, D.; Soyama, H.; De Silva, C. Use of cavitation abrasive surface finishing to improve the fatigue properties of additive manufactured titanium alloy Ti6Al4V. *SAE Technical Papers* **2021**, DOI:10.4271/2021-01-0024.
15. Khajehmirza, H.; Heydari Astaraee, A.; Monti, S.; Guagliano, M.; Bagherifard, S. A hybrid framework to estimate the surface state and fatigue performance of laser powder bed fusion materials after shot peening. *Appl. Surf. Sci.* **2021**, 567, 150758.
16. Maleki, E.; Bagherifard, S.; Razavi, N.; Bandini, M.; du Plessis, A.; Berto, F.; Guagliano, M. On the efficiency of machine learning for fatigue assessment of post-processed additively manufactured AlSi10Mg. *Int. J. Fatigue* **2022**, 160, 106841.
17. Maleki, E.; Bagherifard, S.; Guagliano, M. Correlation of residual stress, hardness and surface roughness with crack initiation and fatigue strength of surface treated additive manufactured AlSi10Mg: Experimental and machine learning approaches. *Journal of Materials Research and Technology* **2023**, 24, 3265-3283.
18. Zhang, C.; Zhu, H.; Liao, H.; Cheng, Y.; Hu, Z.; Zeng, X. Effect of heat treatments on fatigue property of selective laser melting AlSi10Mg. *Int. J. Fatigue* **2018**, 116, 513-522.
19. Romano, S.; Brückner-Foit, A.; Brandão, A.; Gumpinger, J.; Ghidini, T.; Beretta, S. Fatigue properties of AlSi10Mg obtained by additive manufacturing: Defect-based modelling and prediction of fatigue strength. *Eng. Fract. Mech.* **2018**, 187, 165-189.
20. Qian, G.; Jian, Z.; Qian, Y.; Pan, X.; Ma, X.; Hong, Y. Very-high-cycle fatigue behavior of AlSi10Mg manufactured by selective laser melting: Effect of build orientation and mean stress. *Int. J. Fatigue* **2020**, 138, 105696.
21. Beretta, S.; Gargourimotlagh, M.; Foletti, S.; du Plessis, A.; Riccio, M. Fatigue strength assessment of "as built" AlSi10Mg manufactured by SLM with different build orientations. *Int. J. Fatigue* **2020**, 139, 105737.

22. Lehner, P.; Blinn, B.; Beck, T. Improving the defect tolerance and fatigue strength of am AlSi10Mg. *Adv. Eng. Mater.* **2023**, 25, DOI: 10.1002/adem.202201855
23. Bagherifard, S.; Beretta, N.; Monti, S.; Riccio, M.; Bandini, M.; Guagliano, M. On the fatigue strength enhancement of additive manufactured AlSi10Mg parts by mechanical and thermal post-processing. *Mater. Des.* **2018**, 145, 28-41.
24. Uzan, N.E.; Ramati, S.; Shneck, R.; Frage, N.; Yeheskel, O. On the effect of shot-peening on fatigue resistance of AlSi10Mg specimens fabricated by additive manufacturing using selective laser melting (AM-SLM). *Addit. Manuf.* **2018**, 21, 458-464.
25. Maleki, E.; Bagherifard, S.; Sabouri, F.; Bandini, M.; Guagliano, M. Hybrid thermal, mechanical and chemical surface post-treatments for improved fatigue behavior of laser powder bed fusion AlSi10Mg notched samples. *Surface and Coatings Technology* **2022**, 430, 127962.
26. Nakamura, M.; Takahashi, K.; Saito, Y. Effect of shot and laser peening on fatigue strength of additively manufactured aluminum alloy with rough surfaces. *J. Mater. Eng. Perform.* **2022**, 32, 1589-1600.
27. Maleki, E.; Bagherifard, S.; Unal, O.; Sabouri, F.; Bandini, M.; Guagliano, M. Effects of different mechanical and chemical surface post-treatments on mechanical and surface properties of as-built laser powder bed fusion AlSi10Mg. *Surface and Coatings Technology* **2022**, 439, 128391.
28. Maleki, E.; Bagherifard, S.; Unal, O.; Bandini, M.; Guagliano, M. On the effects of laser shock peening on fatigue behavior of V-notched AlSi10Mg manufactured by laser powder bed fusion. *Int. J. Fatigue* **2022**, 163, 107035.
29. Maleki, E.; Bagherifard, S.; Unal, O.; Jam, A.; Shao, S.; Guagliano, M.; Shamsaei, N. Superior effects of hybrid laser shock peening and ultrasonic nanocrystalline surface modification on fatigue behavior of additive manufactured AlSi10Mg. *Surface and Coatings Technology* **2023**, 463, 129512.
30. Biddlecom, J.; Li, Y.; Zhao, X.; Berfield, T.A.; Pataky, G.J. Femtosecond laser shock peening residual stress and fatigue life of additive manufactured AlSi10Mg. *JOM* **2023**, 75, 1964-1974.
31. Maleki, E.; Bagherifard, S.; Heydari Astaraee, A.; Sgarbazzini, S.; Bandini, M.; Guagliano, M. Application of gradient severe shot peening as a novel mechanical surface treatment on fatigue behavior of additively manufactured AlSi10Mg. *Materials Science and Engineering: A* **2023**, 881, 145397.
32. Maleki, E.; Bagherifard, S.; Unal, O.; Revuru, M.; Bandini, M.; Guagliano, M. The efficiency of tumble finishing as a final post-treatment for fatigue enhancement of notched laser powder bed fusion AlSi10Mg. *Sci Rep* **2023**, 13, 4602.
33. Peyre, P.; Fabbro, R.; Merrien, P.; Lieurade, H.P. Laser shock processing of aluminium alloys. Application to high cycle fatigue behaviour. *Mater. Sci. Eng. A.* **1996**, 210, 102-113.
34. Hatamleh, O.; Lyons, J.; Forman, R. Laser and shot peening effects on fatigue crack growth in friction stir welded 7075-T7351 aluminum alloy joints. *Int. J. Fatigue* **2007**, 29, 421-434.
35. Luong, H.; Hill, M.R. The effects of laser peening and shot peening on high cycle fatigue in 7050-T7451 aluminum alloy. *Mater. Sci. Eng. A* **2010**, 527, 699-707.
36. Trdan, U.; Skarba, M.; Grum, J. Laser shock peening effect on the dislocation transitions and grain refinement of Al–Mg–Si alloy. *Mater. Charact.* **2014**, 97, 57-68.
37. Lu, J.; Lu, H.; Xu, X.; Yao, J.; Cai, J.; Luo, K. High-performance integrated additive manufacturing with laser shock peening –induced microstructural evolution and improvement in mechanical properties of ti6al4v alloy components. *International Journal of Machine Tools and Manufacture* **2020**, 148, 103475.
38. Zhang, Y.; Guo, W.; Shi, J.; Chi, J.; Chen, G.; Han, G.; Zhang, H. Improved rotating bending fatigue performance of laser directed energy deposited Ti6Al4V alloys by laser shock peening. *Journal of Alloys and Compounds* **2024**, 980, 173664.
39. Stránský, O.; Beránek, L.; Pathak, S.; Šmaus, J.; Kopeček, J.; Kaufman, J.; Böhm, M.; Brajer, J.; Mocek, T.; Holešovský, F. Effects of sacrificial coating material in laser shock peening of L-PBF printed AlSi10Mg. *Virtual Phys. Prototyp.* **2024**, 19, DOI:10.1080/17452759.2024.2340656.
40. Gong, Z.; Zhang, T.; Chen, Y.; Lu, J.; Ding, X.; Zhang, S.; Lan, M.; Shen, Y.; Wang, S. Effect of laser shock peening on stress corrosion cracking of TC4/2A14 dissimilar metal friction stir welding joints. *Journal of Materials Research and Technology* **2024**, 30, 1716-1725.
41. Liu, Q.; Chu, S.; Zhang, X.; Wang, Y.; Zhao, H.; Zhou, B.; Wang, H.; Wu, G.; Mao, B. Laser shock processing of titanium alloys: A critical review on the microstructure evolution and enhanced engineering performance. *J. Mater. Sci. Technol.* **2025**, 209, 262-291.
42. Sano, Y.; Mukai, N.; Okazaki, K.; Obata, M. Residual stress improvement in metal surface by underwater laser irradiation. *Nucl. Instrum. Methods Phys. Res. Sect. B-Beam Interact. Mater. Atoms* **1997**, 121, 432-436.
43. Sano, Y.; Obata, M.; Kubo, T.; Mukai, N.; Yoda, M.; Masaki, K.; Ochi, Y. Retardation of crack initiation and growth in austenitic stainless steels by laser peening without protective coating. *Materials Science and Engineering A* **2006**, 417, 334-340.
44. Sano, T.; Eimura, T.; Hirose, A.; Kawahito, Y.; Katayama, S.; Arakawa, K.; Masaki, K.; Shiro, A.; Shobu, T.; Sano, Y. Improving fatigue performance of laser-welded 2024-T3 aluminum alloy using dry laser peening. *Metals* **2019**, 9, 1192.

45. Sano, Y. Quarter century development of laser peening without coating. *Metals* **2020**, 10, 152.
46. Sano, Y.; Kato, T.; Mizuta, Y.; Tamaki, S.; Yokofujita, K.; Taira, T.; Hosokai, T.; Sakino, Y. Development of a portable laser peening device and its effect on the fatigue properties of HT780 butt-welded joints. *Forces in Mechanics* **2022**, 7, 100080.
47. Kato, T.; Sakino, Y.; Sano, Y. Effect of laser peening without coating (LPwC) on retardation of fatigue crack growth in SM490 plates. *Forces in Mechanics* **2023**, 13, 100234.
48. Sano, Y.; Akita, K.; Sano, T. A mechanism for inducing compressive residual stresses on a surface by laser peening without coating. *Metals* **2020**, 10, 816.
49. Sasoh, A.; Watanabe, K.; Sano, Y.; Mukai, N. Behavior of bubbles induced by the interaction of a laser pulse with a metal plate in water. *Applied Physics A* **2005**, 80, 1497-1500.
50. Soyama, H. Comparison between the improvements made to the fatigue strength of stainless steel by cavitation peening, water jet peening, shot peening and laser peening. *J. Mater. Process. Technol.* **2019**, 269, 65-78.
51. Soyama, H.; Korsunsky, A.M. A critical comparative review of cavitation peening and other surface peening methods. *J. Mater. Process. Technol.* **2022**, 305, 117586.
52. Leuders, S.; Thone, M.; Riemer, A.; Niendorf, T.; Troster, T.; Richard, H.A.; Maier, H.J. On the mechanical behaviour of titanium alloy TiAl6V4 manufactured by selective laser melting: Fatigue resistance and crack growth performance. *Int. J. Fatigue* **2013**, 48, 300-307.
53. Masuo, H.; Tanaka, Y.; Morokoshi, S.; Yagura, H.; Uchida, T.; Yamamoto, Y.; Murakami, Y., Effects of defects, surface roughness and hip on fatigue strength of Ti-6A1-4V manufactured by additive manufacturing, 3rd International Symposium on Fatigue Design and Material Defects (FDMD), Lecco, ITALY, 2017, 19-26, DOI:10.1016/j.prostr.2017.11.055.
54. Sun, Y.Y.; Lu, S.L.; Gulizia, S.; Oh, C.H.; Fraser, D.; Leary, M.; Qian, M. Fatigue performance of additively manufactured Ti-6Al-4V: Surface condition vs. Internal defects. *JOM* **2020**, 72, 1022-1030.
55. Tarik Hasib, M.; Ostergaard, H.E.; Li, X.; Kruzic, J.J. Fatigue crack growth behavior of laser powder bed fusion additive manufactured Ti-6Al-4V: Roles of post heat treatment and build orientation. *Int. J. Fatigue* **2021**, 142, 105955.
56. Mishurova, T.; Artzt, K.; Rehmer, B.; Haubrich, J.; Ávila, L.; Schoenstein, F.; Serrano-Munoz, I.; Requena, G.; Bruno, G. Separation of the impact of residual stress and microstructure on the fatigue performance of LPBF Ti-6Al-4V at elevated temperature. *Int. J. Fatigue* **2021**, 148, 106239.
57. du Plessis, A.; Razavi, N.; Wan, D.; Berto, F.; Imdaadulah, A.; Beamer, C.; Shipley, J.; MacDonald, E. Fatigue performance of shelled additively manufactured parts subjected to hot isostatic pressing. *Addit. Manuf.* **2022**, 51, 102607.
58. Guennec, B.; Hattal, A.; Hocini, A.; Mukhtarova, K.; Kinoshita, T.; Horikawa, N.; Gubicza, J.; Djemaï, M.; Dirras, G. Fatigue performance of zirconia-reinforced Ti-6Al-4V nanocomposite processed by laser powder bed fusion: An improvement by hot isostatic pressing. *Int. J. Fatigue* **2022**, 164, 107129.
59. Bhandari, L.; Gaur, V. Different post-processing methods to improve fatigue properties of additively built Ti-6Al-4V alloy. *Int. J. Fatigue* **2023**, 176, 107850.
60. Chern, A.H.; Nandwana, P.; Yuan, T.; Kirka, M.M.; Dehoff, R.R.; Liaw, P.K.; Duty, C.E. A review on the fatigue behavior of Ti-6Al-4V fabricated by electron beam melting additive manufacturing. *Int. J. Fatigue* **2019**, 119, 173-184.
61. Soyama, H.; Kuji, C.; Liao, Y. Comparison of the effects of submerged laser peening, cavitation peening and shot peening on the improvement of the fatigue strength of magnesium alloy az*Journal of Magnesium and Alloys* **2023**, 11, 1592-1607.
62. Soyama, H.; Kuji, C. Improving effects of cavitation peening, using a pulsed laser or a cavitating jet, and shot peening on the fatigue properties of additively manufactured titanium alloy ti6al4v. *Surface and Coatings Technology* **2022**, 451, 129047.
63. Soyama, H.; Tanaka, M.; Takiguchi, T.; Yamamoto, M. Development of a cavitation generator mimicking pistol shrimp. *Biomimetics* **2024**, 9, 47.
64. Soyama, H.; Liang, X.; Yashiro, W.; Kajiwara, K.; Asimakopoulou, E.M.; Bellucci, V.; Birnsteinova, S.; Giovanetti, G.; Kim, C.; Kirkwood, H.J.; Koliyadu, J.C.P.; Letrun, R.; Zhang, Y.; Ulicny, J.; Bean, R.; Mancuso, A.P.; Villanueva-Perez, P.; Sato, T.; Vagovic, P.; Eakins, D.; Korsunsky, A.M. Revealing the origins of vortex cavitation in a venturi tube by high speed x-ray imaging. *Ultrason Sonochem* **2023**, 101, 106715.
65. Blanken, J.; De Moor, R.J.G.; Meire, M.; Verdaasdonk, R. Laser induced explosive vapor and cavitation resulting in effective irrigation of the root canal. Part 1: A visualization study. *Lasers Surg. Med.* **2009**, 41, 514-519.
66. Matsumoto, H.; Yoshimine, Y.; Akamine, A. Visualization of irrigant flow and cavitation induced by Er:YAG laser within a root canal model. *J. Endod.* **2011**, 37, 839-843.
67. Lukac, N.; Jezersek, M. Amplification of pressure waves in laser-assisted endodontics with synchronized delivery of Er:YAG laser pulses. *Lasers Med. Sci.* **2018**, 33, 823-833.

68. Sugimoto, Y.; Obata, S. Behavior of a sphere caused by pulsed laser induced bubble simulating stone crushing with tul. *Proceedings of 11th International Symposium on Cavitation* **2021**, 614-617.
69. Soyama, H. Development of laser cavitation peening using a normal-oscillation Nd:YAG laser. *Coatings* **2023**, 13, 1395.
70. SAE J442 Test strip, holder, and gage for shot peening. *SAE International Standards* **2013**, 1-5.
71. SAE J443 Procedures for using standard shot peening almen strip. *SAE International Standards* **2010**, 1-6.
72. Soyama, H.; Iga, Y. Laser cavitation peening: A review. *Applied Sciences* **2023**, 13, 6702.
73. Ward, B.; Emmony, D.C. The energies and pressures of acoustic transients associated with optical cavitation in water. *J. Mod. Opt.* **1990**, 37, 803-811.
74. Ohl, C.D.; Lindau, O.; Lauterborn, W. Luminescence from spherically and aspherically collapsing laser induced bubbles. *Phys. Rev. Lett.* **1998**, 80, 393-396.
75. Lauterborn, W.; Ohl, C.D. Cavitation bubble dynamics. *Ultrason. Sonochem.* **1997**, 4, 65-75.
76. Ohl, C.D.; Kurz, T.; Geisler, R.; Lindau, O.; Lauterborn, W. Bubble dynamics, shock waves and sonoluminescence. *Philos. Trans. R. Soc. A-Math. Phys. Eng. Sci.* **1999**, 357, 269-294, DOI: 10.1098/rsta.1999.0327.
77. Rayleigh, L. On the pressure developed in a liquid during the collapse of a spherical cavity. *The London, Edinburgh, and Dublin Philosophical Magazine and Journal of Science* **1917**, 34, 94-98.
78. Little, R.E. Estimating the median fatigue limit for very small up-and-down quantal response tests and for S-N data with runouts. *ASTM STP* **1972**, 511, 29-42.
79. He, B.B. Two-dimensional X-ray diffraction. *John Wiley & Sons, Inc., New Jersey* **2009**, 249-328.
80. ISO 21920-2, I. Geometrical product specifications (gps) — surface texture: Profile, part 2: Terms, definitions and surface texture parameters. *ISO* **2021**.
81. Linder, J.; Axelsson, M.; Nilsson, H. The influence of porosity on the fatigue life for sand and permanent mould cast aluminium. *Int. J. Fatigue* **2006**, 28, 1752-1758.
82. Taylor, J.R., An introduction to error analysis, the study of uncertainties in physical measurements, University Science Books, **1982**.